An Image Processing Approach to Wideband Spectrum Sensing of Heterogeneous Signals

Ha Q. Nguyen(✉), Ha P. K. Nguyen, and Binh T. Nguyen

Viettel Research and Development Institute, Hoa Lac High-tech Park, Hanoi, Vietnam
nguyenquyha@gmail.com, khanhha318@gmail.com, thaibinhnx@gmail.com

Abstract. We introduce a simple yet efficient framework for the localization and tracking of fixed-frequency and frequency-hopping (FH) wireless signals that coexist in a wide radio-frequency band. In this spectrum sensing scheme, an energy detector is applied to each Short-time Fourier Transform of the wideband signal to produce a binary spectrogram. Bounding boxes for narrowband signals are then identified by using image processing techniques on a block of the spectrogram at a time. These boxes are also tracked along the time axis and fused with the newly detected boxes to provide an on-line system for spectrum sensing. Fast and highly accurate detection is achieved in simulations for various FF signals and FH signals with different hopping patterns and speeds. In particular, for the SNR of 4 dB over a bandwidth of 50 MHz, 97.98% of narrowband signals were detected with average deviations of about 0.02 ms in time and 2.15 KHz in frequency.

Keywords: Wideband spectrum sensing · Wireless signal detection
Frequency hopping · Time-frequency analysis · Spectrogram
Waterfall image · Image morphology · Blob extraction

1 Introduction

Spectrum sensing is the central task of any cognitive radio networks [6,8], since it provides a continuing surveillance for better utilization of the radio spectrum. Various methods have been proposed for the narrowband spectrum sensing (NSS) [14], which detects the presence of wireless signals in each frequency subband. However, the local spectrum information provided by the NSS is deficient for the decision making of cognitive nodes in the network. Furthermore, the division of the radio spectrum into subbands are often too coarse to precisely identify all narrowband signals. Because of these shortcomings of NSS, considerable attention has recently been shifted to the wideband spectrum sensing (WSS) [10], which investigates the whole spectrum of interest at a time. The main challenge of WSS lies at the extremely-high sampling frequency, which

I. Moerman et al. (Eds.): CROWNCOM 2018, LNICST 261, pp. 211–221, 2019.
https://doi.org/10.1007/978-3-030-05490-8_20

has to be greater or equal to the bandwidth of the wideband signal, according to Shannon's theory. To ease this burden for the Analog-to-Digital Converter (ADC), a large body of literature [1,2,7,12,15] has focused on the sub-Nyquist sampling (a.k.a. compressive sampling) techniques for WSS. Existing methods for *signal detection*–the core of WSS–often rely on the detection of irregularities in the Power Spectrum Density (PSD) [3,11–13]. This 1-D approach yields accurate localization of the frequency subbands in every single time slot but, unfortunately, does not keep track of the evolution of narrowband signals over time. Another drawback of the 1-D detection algorithms is that they need to be repeated for every (short) time slot, leading to heavy computation that prevents them from real-time implementations.

In this paper, we propose a 2-D approach to WSS in which the signal localization is obtained by applying image processing techniques to a *block* of *binary* spectrogram that is a concatenation of multiple thresholded PSDs. The thresholding of PSDs, or energy detection, is done via a noise floor estimation algorithm proposed in [9], which is also based on image processing. The detected signals are then tracked across a waterfall of time-frequency images and associated with bounding boxes on the spectrogram to form an on-line detection system. Most importantly, the proposed scheme is able to simultaneously handle fixed-frequency (FF) and frequency-hopping (FH) signals that might be transmitted at the same time over a wideband spectrum. These 2 types of signals differ mainly by the time duration: a single hop of an FH signal is typically much shorter than an FF signal. Therefore, it requires a sufficiently long observation to distinguish one type of signal from the other. The benefits of our framework are twofold. First, unlike 1-D detection methods, the proposed mechanism provides a dynamic localization of the narrowband signals in both time and frequency. Second, the computation can be made very fast by amortizing the processing of a binary image over a certain period of time. Our WSS system can also be linked to the time-frequency analysis methods that are widely used in speech and acoustics processing [5].

The outline of the rest of the paper is as follows: Sect. 2 describes the building blocks of our spectrum sensing system; Sect. 3 reports some detection results on simulated data; and Sect. 4 concludes the paper.

2 Architecture of the Proposed System

Notation: Throughout this section, images are denoted by bold letters. For image $\boldsymbol{I}$, we use the notation $I(x, y)$ to refer to the pixel value at row y and column x.

As shown in Fig. 1, the proposed scheme consists of 3 main modules: Spectrogram Binarization, Signal Localization, and Signal Tracking. The input to the system is a wideband analog signal $s(t)$ that is a (noisy) superposition of multiple narrowband signals inside the frequency band $[0, B_{\text{wide}}]$. The output of the system is a list of bounding boxes that dynamically localize all narrowband signals appearing in the time-frequency *waterfall* image (or spectrogram) of the input signal. See Fig. 7 for a visualization of the desired result: FF and FH signals

are tightly surrounded by red and green boxes, respectively. Each bounding box has 4 vertices lying on the *integer* grid of the time-frequency image and is represented by a tuple (x, y, w, h), where (x, y) are the coordinates of the upper-left corner and (w, h) are the width and height, respectively. The 4 characteristics of a narrowband signal, namely, starting time, stopping time, center frequency, and bandwidth, are computed from its bounding box (x, y, w, h) as

$$t_{\text{start}} = y \times L/B_{\text{wide}}, \quad t_{\text{stop}} = (y + h) \times L/B_{\text{wide}}, \tag{1}$$

$$f_{\text{center}} = (x + w/2) \times B_{\text{wide}}/L, \quad B_{\text{narrow}} = w \times B_{\text{wide}}/L, \tag{2}$$

where L is the size of the window used in computing the spectrogram. In the sequel, we discuss the 3 modules of the system in detail.

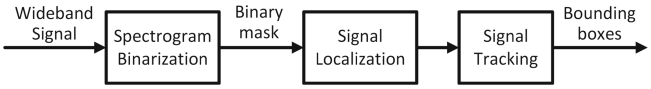

Fig. 1. Building blocks of the proposed system for wideband spectrum sensing.

2.1 Spectrogram Binarization

This module is illustrated in Fig. 2. The analog signal $s(t)$ is first sampled by the ADC (Analog-to-Digital Converter) at Nyquist's rate:

$$s[n] = s\left(n/B_{\text{wide}}\right), \quad n = 0, 1, 2, \ldots$$

Then, finite-length signals are obtained by sliding a window $w[n]$ of size L along $s[n]$. In particular, for $m \geq 0$, we define windowed signals s_m as

$$s_m[n] = w[n] \cdot s[mL + n], \quad \text{for } n = 0, \ldots, L - 1.$$

Next, the PSD (Power Spectrum Density) of each signal block is computed via the FFT (Fast Fourier Transform) as

$$P_m[k] = 10 \log_{10} \left| \sum_{n=0}^{L-1} s_m[n] \mathrm{e}^{-\frac{\mathrm{j}2\pi kn}{L}} \right|^2, \quad \text{for } k = 0, \ldots, L - 1.$$

This windowed Fourier transform is also known as Short-time Fourier Transform (STFT). Using the above PSD, a noise floor $F_m[k]$ is estimated by a morphology-based algorithm proposed in [9].[1]

[1] In practice, due to the slow variation of the noise with time, the noise floor estimation can be done once for multiple signal blocks.

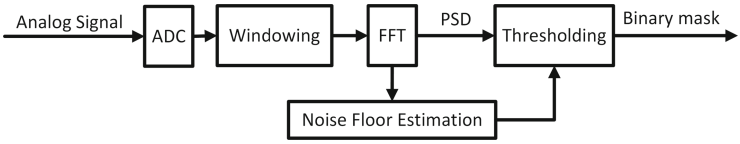

Fig. 2. Block diagram of the Spectrogram Binarization module.

The final step of the Spectrogram Binarization is to obtain binary masks $\{X_m\}_{m\geq 0}$ according to the thresholding

$$X_m[k] = \begin{cases} 1, & \text{if } P_m[k] > F_m[k] + T_{\text{offset}} \\ 0, & \text{otherwise,} \end{cases}$$

where T_{offset} (dB) is a hyper-parameter. Stacking these binary masks together yields a waterfall image of L columns and undefined number of rows. The horizontal and vertical axes of the image represent frequency and time, respectively.

2.2 Signal Localization

In this module, we extract M consecutive rows of the waterfall image obtained from the previous stage and identify the narrowband signal blobs inside it. As illustrated in Fig. 3, this function takes a binary image $\boldsymbol{I}$ of size $M \times L$ and outputs 2 box lists $\mathcal{F}$ and $\mathcal{H}$ for FF and FH signals, respectively. The main routines of the Signal Localization module are described below.

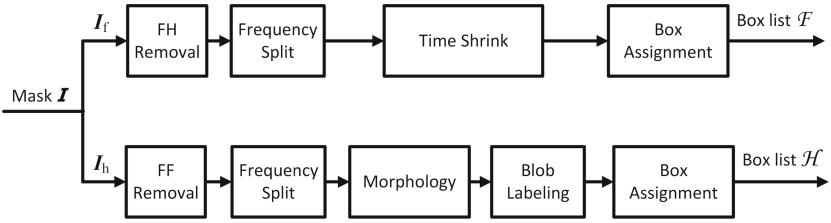

Fig. 3. Block diagram of the Signal Localization module.

Localization of FF Signals (Upper Branch)

1. *Initialize* $\boldsymbol{I}_{\text{f}} \leftarrow \boldsymbol{I}$.
2. *FH Removal:* This step erases FH signals out of the image $\boldsymbol{I}_{\text{f}}$ by setting

$$I_{\text{f}}(x, y) \leftarrow 0, \quad \text{if } \sum_{y} I_{\text{f}}(x, y) < T_{\text{f,col}} \times M,$$

where $T_{\text{f,col}} \in (0, 1)$ is a hyper-parameter. Interestingly, this step also helps reduce the noise, which are sporadically distributed in the spectrogram.

3. *Frequency Split:* This step provides a frequency localization for the FF signals. We divide $\boldsymbol{I}_{\mathrm{f}}$ into N_{f} sub-images $\{\boldsymbol{I}_{\mathrm{f}}^{(k)}\}_{k=1}^{N_{\mathrm{f}}}$—strips of columns of $\boldsymbol{I}_{\mathrm{f}}$ that are separated by at least $T_{\mathrm{f},0}$ consecutive zero-columns. After this step, each sub-image supposedly contains a single FF signal. As the output of this step, we also store the indices of the first columns of these sub-images as $\{c_k\}_{k=1}^{N_{\mathrm{f}}}$. Note that $T_{\mathrm{f},0}$ is a hyper-parameter of this routine.
4. *Time Shrink:* The time localization is then performed on each sub-image as

$$I_{\mathrm{f}}^{(k)}(x,y) \leftarrow 0, \quad \text{if } \sum_{x} I_{\mathrm{f}}^{(k)}(x,y) < T_{\mathrm{f,row}} \times L_k,$$

where L_k is the number of columns in the kth sub-image and $T_{\mathrm{f,row}} \in (0,1)$ is a hyper-parameter of this step.
5. *Box Assignment:* This step finally outputs a box list $\mathcal{F} = \{(x_k, y_k, w_k, h_k)\}_{k=1}^{N_{\mathrm{f}}}$ where each box is given by

$$\begin{aligned} x_k &= c_k, \quad w_k = L_k, \\ y_k &= r + \min_{y:\sum_x I_{\mathrm{f}}^{(k)}(x,y)>0} y, \\ h_k &= \max_{y:\sum_x I_{\mathrm{f}}^{(k)}(x,y)>0} y \; - \min_{y:\sum_x I_{\mathrm{f}}^{(k)}(x,y)>0} y + 1. \end{aligned}$$

In the above formulas, c_k is the index of the first column, L_k is the number of columns of the kth sub-image $\boldsymbol{I}_{\mathrm{f}}^{(k)}$, and r is the index of the first row of the whole input image $\boldsymbol{I}$.

Localization of FH Signals (Lower Branch)

1. *Initialize* $\boldsymbol{I}_{\mathrm{h}} \leftarrow \boldsymbol{I}$.
2. *FF Removal:* This step erases FF signals out of the image $\boldsymbol{I}_{\mathrm{h}}$ by setting

$$I_h(x,y) \leftarrow 0, \quad \text{if } \sum_{y} I_{\mathrm{h}}(x,y) > T_{\mathrm{h,col}} \times M,$$

where $T_{\mathrm{h,col}} \in (0,1)$ is a hyper-parameter.
3. *Frequency Split*: Similarly to the upper branch, we split $\boldsymbol{I}_{\mathrm{h}}$ into K_{h} sub-images $\{\boldsymbol{I}_{\mathrm{h}}^{(k)}\}_{k=1}^{K_{\mathrm{h}}}$ that are separated by at least $T_{\mathrm{h},0}$ consecutive zero-columns. However, unlike the Frequency Split for FF signals, each sub-image obtained from this step may contain multiple signal hops. The purpose of this step is actually to reduce the heavy computation incurred by the morphological operators in the next step.
4. *Morphology:* We then apply 2 morphological operators on each sub-image as

$$I_{\mathrm{h}}^{(k)} \leftarrow \left(I_{\mathrm{h}}^{(k)} \bullet E_1\right) \circ E_2,$$

where the symbols $\bullet$ and $\circ$ denote the closing and opening operators [4], respectively; E_1 and E_2 are the corresponding structuring elements. While

the closing operator interpolates the holes in each hop, the opening operator plays the role of a denoiser. In experiments, we always choose E_1 and E_2 to be rectangle structuring elements of size $|E_1|$ and $|E_2|$, respectively, which are the hyper-parameters of this step. Figure 4 illustrates the effect of the Morphology procedure.

5. *Blob Labeling:* This step extracts the time-frequency hops by applying a connected-component labeling algorithm on each of the sub-images. The output of this step is a list of sets $\{\mathcal{S}_k\}_{k=1}^{N_\mathrm{h}}$ where each set $\mathcal{S}_k$ contains the coordinates (x, y) of 4-connected pixels of value 1.
6. *Box Assignment:* This step gives a box list $\mathcal{H} = \{(x_k, y_k, w_k, h_k)\}_{k=1}^{N_\mathrm{h}}$ where

$$x_k = c_n + \min_{x \in \mathcal{S}_k} x, \quad w_k = \max_{x \in \mathcal{S}_k} x - \min_{x \in \mathcal{S}_k} x + 1,$$
$$y_k = r + \min_{y \in \mathcal{S}_k} y, \quad h_k = \max_{y \in \mathcal{S}_k} y - \min_{y \in \mathcal{S}_k} y + 1.$$

Here, c_n is the index of the first column of the nth sub-image $\boldsymbol{I}_\mathrm{h}^{(n)}$ that contains blob $\mathcal{S}_k$, and r is the index of the first row of the whole image $\boldsymbol{I}$.

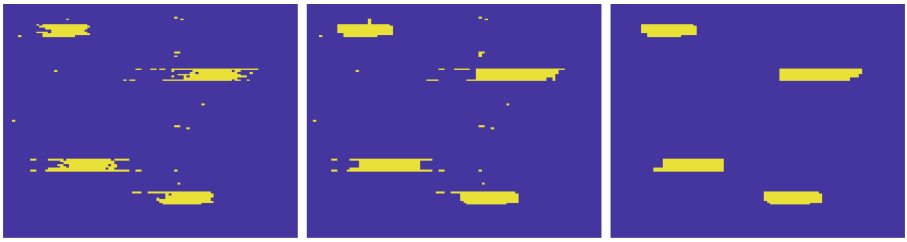

(a) original (b) after closing (c) after opening

Fig. 4. Morphological operators applied to part of the binary spectrogram containing several signal hops.

2.3 Signal Tracking

This module deals with the tracking of signals along the time axis. To that end, we divide the waterfall image into blocks $\{\boldsymbol{I}_n\}_{n \geq 1}$ such that each block has M rows and every 2 consecutive blocks overlap by N_overlap rows. Each block $\boldsymbol{I}_n$ is then passed to the Signal Localization module to obtain 2 box lists $(\mathcal{F}_n, \mathcal{H}_n)$. These two lists are then combined with the previous lists to create 2 new lists $(\mathcal{F}'_n, \mathcal{H}'_n)$ that track all the narrowband signals up to time $t_n = n(M - N_\mathrm{overlap}) + N_\mathrm{overlap}$. The overall tracking procedure is diagrammed in Fig. 5. The 2 main routines of this module are discussed below.

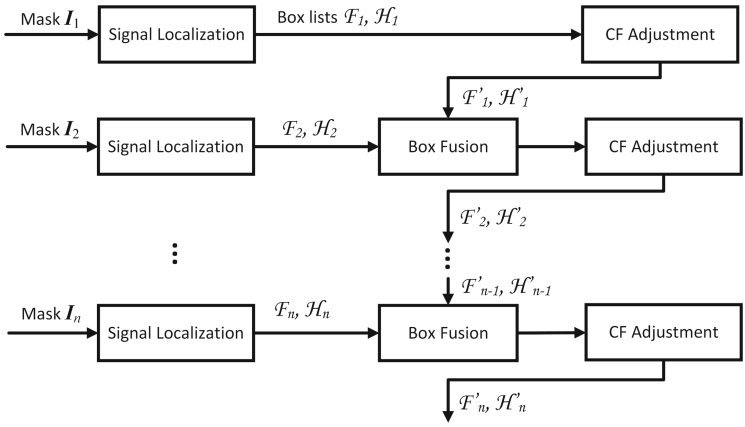

Fig. 5. Block diagram of the Signal Tracking.

1. *CF Adjustment:* In this routine, each bounding box of a narrowband signal is expanded such that the vertical center line (center frequency) of the box contains a significant number of nonzero pixels. Specifically, for a box (x, y, w, h) surrounding a signal, define image $\boldsymbol{I}$ to be the restriction of the spectrogram on the region inside this box. The (x, w) components of the box are then adjusted as

$$x_0 = \underset{x:\sum_y I(x,y) > T_{\text{center}} \times h}{\arg\min} |x - w/2|,$$

$$(x, w) \leftarrow \begin{cases} (x, 2x_0 + 1), & \text{if } x_0 > w/2 \\ (x + 2x_0 - w + 1, 2(w - x_0) - 1), & \text{if } x_0 < w/2. \end{cases}$$

   Here, $T_{\text{center}} \in (0, 1)$ is a hyper-parameter of this step.
2. *Box Fusion:* This routine merges a newly detected box (x, y, w, h) with an existing box (x', y', w', h') in the previous list if the following conditions

$$y - (y' + h) > T_{\text{gap}},$$
$$\min\{x + w, x' + w'\} - \max\{x, x'\} > T_{\text{ratio}} \times \min\{w, w'\}$$

   hold. We use different sets of hyper-parameters: $(T_{\text{f,gap}}, T_{\text{f,ratio}})$ for FF signals and $(T_{\text{h,gap}}, T_{\text{h,ratio}})$ for FH signals. The merged box is then defined as

$$w' \leftarrow \max\{x + w, w' + x'\} - \min\{x, x'\},$$
$$h' \leftarrow \max\{y + h, y' + h'\} - \min\{y, y'\},$$
$$x' \leftarrow \min\{x, x'\}, \quad y' \leftarrow \min\{y, y'\}.$$

The overall effect of the Signal Tracking module is illustrated in Fig. 6.

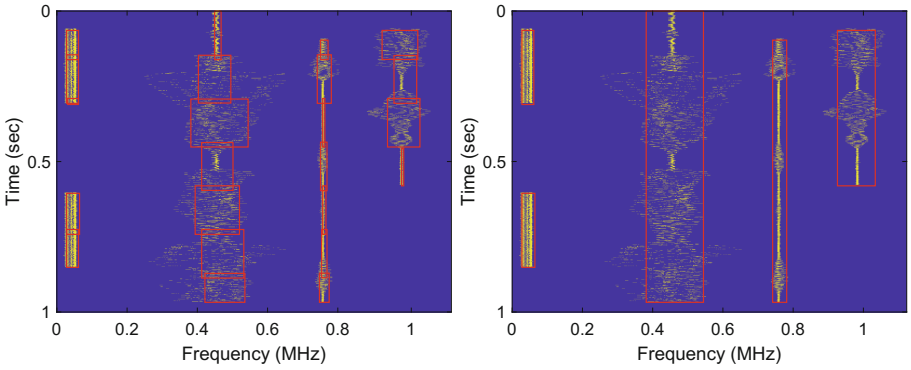

(a) Without tracking (b) With tracking

Fig. 6. Signal Tracking with box fusion and center-frequency adjustment.

3 Numerical Results

The proposed sensing scheme was implemented in Matlab 2017b. We simulated 1 s of a 50 MHz-wideband signal in the spectrum $40 \div 90$ MHz, which produces 50×10^6 samples. This wideband signal contains 43 different narrowband FF signals using Frequency Modulation (FM), a collection of 200 FH signals hopping linearly at speed 200 hops/sec, and another collection of 500 FH signals hopping randomly at speed 500 hops/sec. That results in a total number of 743 signals. For computing the spectrogram, we used a rectangular window of size $L = 2^{14}$. The wideband signal was corrupted by Additive White Gaussian Noise with various levels of Signal-to-Noise Ratio (SNR).

Each binary image going through the Signal Localization module consists of $M = 500$ rows of the spectrogram and overlaps by $N_{\text{overlap}} = 50$ rows with the next image. The other hyper-parameters used in experiments are given in Table 1. The blob labeling was done via the built-in function `bwconncomp` of Matlab. Results are visualized in Fig. 7 with zoomed-in parts of the simulated frequency band. Out of the drawn bounding boxes, we assigned one to a narrowband signal if it overlaps significantly with the ground-truth bounding box. More precisely, the two boxes are matched if the ratio Intersection Over Union (IOU) between them is above 60%. A signal is called *detected* if it is assigned to a bounding box output by the spectrum sensing system. The detection rate and the Mean Absolute Error (MAE) of 4 characteristics of the detected signals, computed by (1) and (2), are reported in Table 2 for 5 different noise levels. It can be seen that the proposed scheme achieved both high detection rate and high accuracy across a relatively wide range of SNRs.

Table 1. Hyper-parameter values. 'SB' stands for Spectrogram Binarization.

Module	SB	Signal localization							Signal tracking				
Param	T_{offset}	$T_{\text{f,col}}$	$T_{\text{f},0}$	$T_{\text{f,row}}$	$T_{\text{h,col}}$	$T_{\text{h},0}$	$\lvert E_1 \rvert$	$\lvert E_2 \rvert$	T_{center}	$T_{\text{f,gap}}$	$T_{\text{f,ratio}}$	$T_{\text{h,gap}}$	$T_{\text{h,ratio}}$
Value	17	0.07	5	0.05	0.2	50	$(2, 4)$	$(2, 2)$	0.6	200	0.3	0	0.7

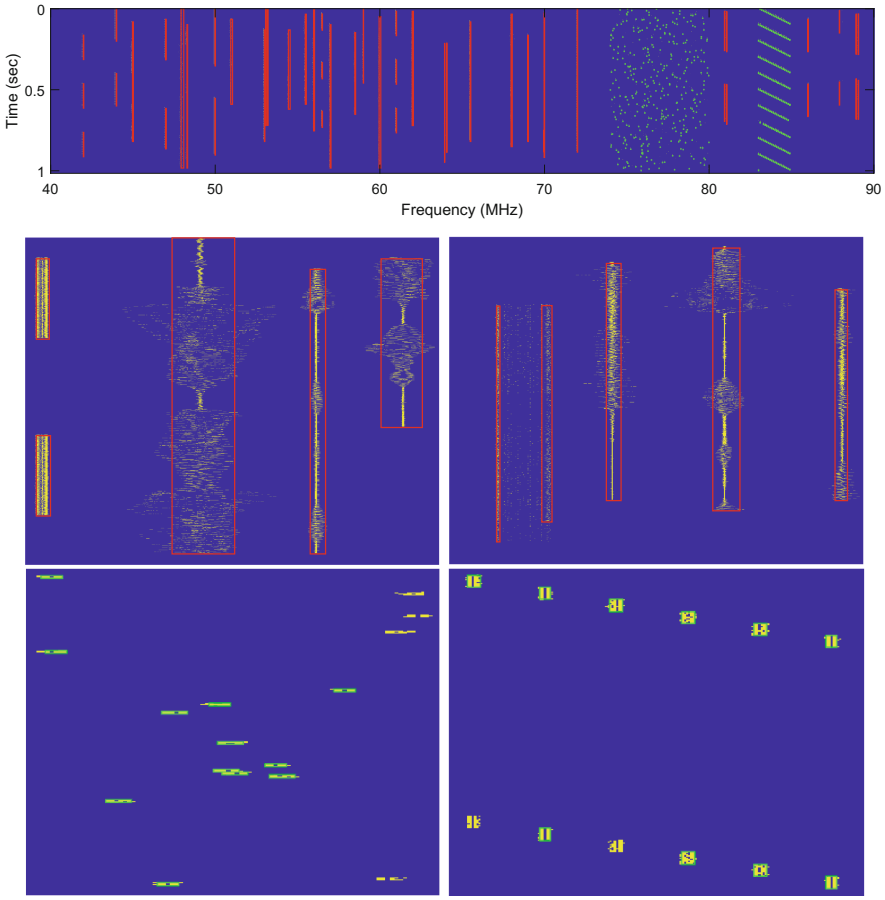

Fig. 7. Top: bounding boxes for FF and FH signals are drawn in red and green, respectively, on binary spectrogram over a bandwidth of 50 MHz and a duration of 1 s with SNR $= -4$ dB. Bottom 4 figures: Zoomed-in subbands. (Color figure online)

Table 2. Detection rate and mean absolute error of 4 characteristics of the detected signals with respect to different SNR levels of the wideband signal.

SNR	Detection rate	Mean absolute error			
		Starting time	Stopping time	Center frequency	Bandwidth
−4 dB	60.43%	0.0882 ms	0.0655 ms	2.4808 KHz	6.8783 KHz
−2 dB	85.87%	0.0649 ms	0.0334 ms	2.3223 KHz	6.2996 KHz
0 dB	94.21%	0.0411 ms	0.0201 ms	2.2278 KHz	5.2229 KHz
2 dB	96.10%	0.0315 ms	0.0155 ms	2.3593 KHz	3.5903 KHz
4 dB	97.98%	0.0272 ms	0.0169 ms	2.3307 KHz	1.9618 KHz

4 Conclusion

We have presented in this paper a novel method for on-line wideband spectrum sensing that relies on the processing and fusion of binary time-frequency images. These images are obtained by combining a simple energy detector with a noise floor estimator on the STFTs of the wideband signal. The signal localization and tracking are both performed on binary images, allowing fast algorithms. As simulations suggested, this method is effective for both fixed-frequency and frequency-hopping signals, which are likely to simultaneously appear in a wide spectrum. We believe that the proposed method can be implemented into a real system for automatic spectrum monitoring, an essential step towards the realization of cognitive radio networks.

References

1. Arianandа, D.D., Leus, G.: Cooperative compressive wideband power spectrum sensing. In: Proceedings of IEEE ASILOMAR, pp. 303–307. Pacific Groove, CA, July 2012
2. Cohen, D., Eldar, Y.C.: Sub-Nyquist sampling for power spectrum sensing in cognitive radios: a unified approach. IEEE Trans. Signal Process. **62**(15), 3897–3910 (2014)
3. Farhang-Boroujeny, B.: Filter bank spectrum sensing for cognitive radios. IEEE Trans. Signal Process. **56**(5), 1801–1811 (2008)
4. Gonzalez, R.C., Woods, R.E.: Digital Image Processing, 3rd edn. Prentice-Hall, Upper Saddle River (2006)
5. Lampert, T.A., O'keefe, S.E.M.: A survey of spectrogram track detection algorithms. Appl. Acoustics **71**(2), 87–100 (2010)
6. Liang, Y.C., Chen, K.C., Li, G.Y., Mahonen, P.: Cognitive radio networking and communications: an overview. IEEE Trans. Veh. Technol. **60**(7), 3386–3407 (2011)
7. Mishali, M., Eldar, Y.C.: Blind multiband signal reconstruction: compressive sensing for analog signals. IEEE Trans. Signal Process. **57**(3), 993–1009 (2009)
8. Mitola, J., Maguire, G.Q.: Cognitive radio: making software radios more personal. IEEE Pers. Commun. **6**(4), 13–18 (1999)
9. Ready, M.J., Downey, M.L., Corbalis, L.J.: Automatic noise floor spectrum estimation in the presence of signals. In: Proceedings of IEEE ASILOMAR, pp. 877–881 (1997)

10. Sun, H., Nallanathan, A., Wang, C.X.: Wideband spectrum sensing for cognitive radio networks: a survey. IEEE Wirel. Commun. **20**(2), 74–81 (2013)
11. Tian, Z., Giannakis, G.B.: A wavelet approach to wideband spectrum sensing for cognitive radios. In: Proceeding of IEEE CROWNCOM, pp. 1–5, Mykonos Island, Greece, 08–10 July 2006
12. Tian, Z., Tafesse, Y., Sadler, B.M.: Cyclic feature detection with sub-Nyquist sampling for wideband spectrum sensing. IEEE J. Sel. Top. Signal Process. **6**(1), 58–69 (2012)
13. Watson, C.M.: Signal detection and digital modulation classification-based spectrum sensing for cognitive radio. Ph.D. thesis, Northeastern University, Boston, MA, USA (2013)
14. Yucek, T., Arslan, H.: A survey of spectrum sensing algorithms for cognitive radio applications. IEEE Commun. Surv. Tutor. **11**(1), 116–130 (2009)
15. Zeng, F., Li, C., Tian, Z.: Distributed compressive spectrum sensing in cooperative multihop cognitive networks. IEEE J. Sel. Top. Signal Process. **5**(1), 37–48 (2011)